Target Motion Estimation Techniques in Single-Channel SAR

Mark T. Crockett

***Abstract*—Synthetic Aperture Radar (SAR) systems are versatile, high-resolution radar imagers useful for providing detailed intelligence, surveillance, and reconnaissance, especially when atmospheric conditions are non-ideal for optical imagers. However, targets in SAR images are smeared when they are moving. Along-track interferometry is a commonly-used method for extracting the motion parameters of moving targets but requires a dual-aperture SAR system, which may be power- size- or cost-prohibitive. This paper presents a method of estimating target motion parameters in single-channel SAR data given geometric target motion constraints. This estimation method includes an initial estimate, computation of the SAR ambiguity function, and application of the target motion constraints.**

I. Introduction

FOR many centuries, the outcome of wars has been decided primarily by the size of opposing military forces. But during the last century, the success of any military effort has become largely dependent on military intelligence. Surveillance can help militaries prepare for and plan attacks and counter attacks by finding weak spots to exploit in the enemy's defense, tracking enemy movement, and finding supply lines. Knowing how targets move can enhance these abilities.

Visual and optical surveillance via manned aircraft were first used in World War I and became part of common military strategy in World War II. Optical imagers can be accurate, low-cost, and provide real-time target acquisition, but they underperform in the presence of clouds, fog, or darkness. Imaging radar provides similar results but its performance is not compromised by poor atmospheric conditions. Traditional imaging radar requires a long antenna to produce a finely-spaced imaging grid, but synthetic aperture radar (SAR) utilizes radar platform motion and a small antenna to synthesize a long antenna aperture in order to produce fine-resolution images.

Similar to optical images, moving targets in SAR images are generally smeared or blurred. If the motion parameters of the target are known, this effect can be alleviated by compensating for target motion. In order to extract these motion parameters, a SAR system may employ along-track interferometry (ATI) by using two antennas separated by a baseline to form two images of the same scene at different times. The images can then be compared for phase differences on a pixel-to-pixel basis, which indicate the presence of moving targets [1].

Recent technological advancements have facilitated the development of small, low-power, low-cost SAR systems which are often found on small unmanned aircraft systems (UAS). In the last ten years, UAS have become quite common in reconnaissance because they are cost-efficient and inherently less risky than manned surveillance aircraft. UAS usually have very tight payload and power restrictions which may prohibit the use of two antennas for ATI. Since single-channel Doppler shift measurements rely on either the target or the observer being stationary, we cannot perform ATI with a single antenna. These conditions motivate us to investigate a practical method for focusing single-channel SAR images of moving targets.

Ground moving target indication (GMTI) is a radar operation mode used to discriminate targets from surrounding clutter. Previous work shows that the GMTI solution of a moving target in single-channel SAR is not unique. A complete GMTI solution requires solving for four parameters (target position in range and azimuth, heading, and speed) but single-channel SAR data has only enough information to solve for three [2]. To address these issues, this paper shows how to constrain the problem sufficiently in order to get the complete GMTI solution for a moving target in single-channel SAR.

This paper is organized as follows. Section II gives an overview of SAR, the geometry that makes it possible, its signal properties, and image processing. In Section III, I discuss the behavior of moving targets in a SAR image, the non-unique nature of moving target signatures in single-channel SAR data, and a SAR ambiguity function. Section IV provides the base of the work in this paper by demonstrating the results of target motion parameter estimation for constant motion using single-channel SAR data. In Section V, I discuss conclusions from this work and future work.

II. Background

A critical factor in evaluating SAR performance is signal-to-noise ratio (SNR). It simply compares the received signal power to the noise power, which interferes with the signal of interest. The SNR of a SAR system can be expressed as

$$SNR = \frac{P_t G^2 \lambda^2 \sigma n_p}{(4\pi)^3 R^4 P_n} \tau \beta, \tag{1}$$

where P_t is the transmitted power, G is the antenna gain, λ is the carrier wavelength, σ is the radar cross-section, n_p is the number of pulses used to image a single pixel, τ is the pulse duration, β is the signal bandwidth, R is the slant range from the radar to a target, and P_n is the receiver noise power [3].

This section provides a background of SAR systems, including their geometry, signal properties, resolution, antenna design, target scattering properties, and image formation. Throughout this section, I also review all of the pertinent terms listed in Eq. (1), which is known as the radar range equation (RRE).

A. SAR Geometry

Synthetic Aperture Radar works as it does primarily because the radar is usually on a moving platform – typically an aircraft or spacecraft. SAR images can often be visualized in terms of "slow time" and "fast time." Slow time refers to an amount of time relating to the coherent processing interval whereas fast time refers to an amount of time on the order of one inter-pulse period, which is generally orders of magnitude less than the inter-pulse period. In this paper, I use "azimuth" to reference the direction of flight (slow time, along-track direction) and "range" to reference the direction orthogonal to the azimuth direction (fast time, cross-track direction).

There are three common types of SAR operation modes: stripmap, spotlight, and scanning. In stripmap mode, the antenna pointing direction (radar line of sight (LOS)) is fixed orthogonal to the azimuth direction or squinted forward or backward. As the aircraft moves along its flight path, the antenna's footprint also moves along the ground at the same velocity. The SAR transmits and receives many pulses for the same point on the ground, but it images a "strip" of ground. In spotlight mode, the antenna moves (using a gimbal or a phased array) so that it remains pointed at the same spot on the ground throughout the data collection. This allows better SNR and resolution because of the longer dwell time on a single area. In scanning SAR, the antenna moves side-to-side in range to increase the width of the imaging swath. This paper focuses exclusively on non-squinted stripmap SAR, as depicted in Fig. 1.

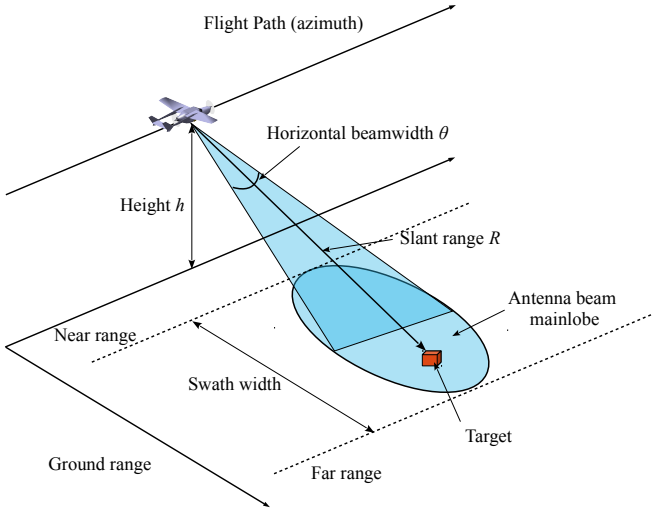

Fig. 1. Stripmap SAR imaging geometry.

Several factors dictate the area of ground to be imaged. The length of time that pulses are successively transmitted and received is called the collection time and determines the length of the image. The desired imaging swath width determines the maximum pulse repetition frequency (PRF) and the unambiguous range. The PRF is given by

$$PRF = \frac{1}{PRI}, \tag{2}$$

where PRI is the pulse repetition interval, which is the amount of time between consecutive transmit pulses. In order to distinguish one received pulse from another, they must not overlap. Therefore, the PRF must be low enough that the echo from the farthest edge of the swath for one pulse is received before the echo from the nearest edge of the swath for the next pulse. The PRF determines the unambiguous range R_{ua}, which is given by [3]

$$R_{ua} = \frac{c}{2PRF}, \tag{3}$$

where c is the speed of electromagnetic wave propagation. That is, R_{ua} is the maximum range at which target echoes are received without interfering. Targets at a range greater than R_{ua} alias to an "apparent range" that is within the imaging swath. Also, since the unambiguous Doppler $f_{d_{ua}}$, or range of Doppler frequencies that can be measured without aliasing is given by [3]

$$f_{d_{ua}} = PRF, \tag{4}$$

the PRF must be as large as the expected range of Doppler shifts observed by the radar. This range of observed Doppler frequencies B_d is

$$B_d = \frac{4v}{\lambda} \sin\left(\frac{\theta_3}{2}\right) \sin\psi, \tag{5}$$

where v is the radar platform velocity, λ is the carrier wavelength, θ_3 is the antenna's azimuth beamwidth, and ψ is the angle between the aircraft velocity vector and the radar LOS [3].

B. Signal Properties

Some radars use continuous-wave (CW) signals, which are pure-frequency signals that have uninterrupted transmission. An interrupted continuous-wave (ICW) signal is just a CW signal with a duty cycle less than 100%. In terms of signal transmission and reception, a SAR system works much like a traditional imaging radar. The earliest forms of SAR used ICW signals, but most now employ some type of linear frequency-modulated (LFM) signal.

Figure 2 shows an example of an ICW signal. It has a constant frequency and a pulse duration τ defined by

$$\tau = d_t \cdot PRI, \tag{6}$$

where d_t is the transmit duty cycle, or the percentage of one pulse period that the signal is transmitting.

By contrast, while an LFM signal is also pulsed, its frequency is linearly swept from low to high or vice versa at the chirp rate k_r. Figure 3 shows a sample LFM signal. In general, radar transmit carrier frequencies range from 300 MHz to about 300 GHz, but for convenience, Figs. 2 and 3 show signals that have been mixed to baseband. As shown in Fig. 3, the signal frequency starts at zero and ramps up to a higher frequency and this pattern repeats for every transmit pulse.

A zero-phase LFM transmit signal $s_t(t)$ can be expressed as [4]

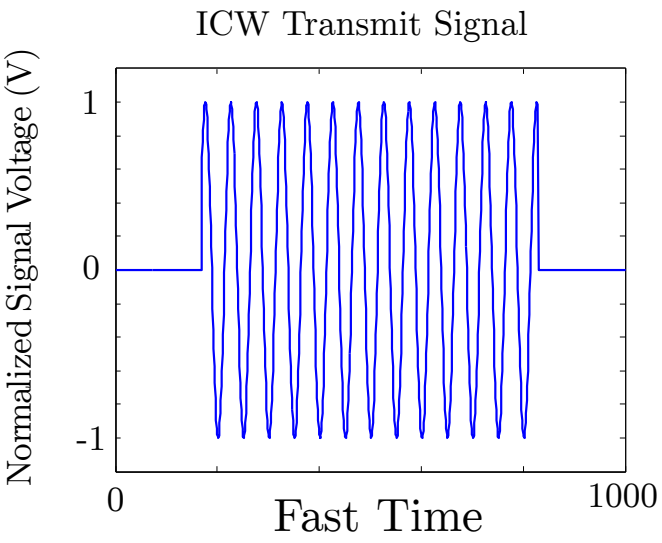

Fig. 2. A rectangular-windowed ICW waveform.

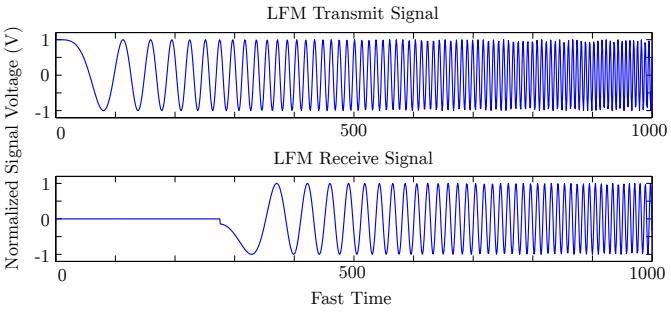

Fig. 3. LFM transmit and receive signals.

$$s_t(t) = A \exp\left(\jmath\left(2\pi f_0 t + \pi k_r t^2\right)\right), \tag{7}$$

where A is the signal amplitude at time t and f_0 is the carrier frequency. The received signal $s_r(t)$ is just an attenuated, time-shifted copy of the transmit signal and is given by

$$s_r(t) = A' \exp\left(\jmath\left(2\pi f_0 (t-\Delta t) + \pi k_r (t-\Delta t)^2\right)\right), \tag{8}$$

where A' is the attenuated signal amplitude and Δt is the two-way time of flight from the radar to a target at range R:

$$\Delta t = \frac{2R}{c}. \tag{9}$$

For convenience in processing, the received signal is usually mixed down to baseband and is given by

$$s_{rmd}(t) = A' \exp\left[\jmath\big(2\pi(f_0 - f_{md})t - 2\pi f_0 \Delta t + \pi k_r (t-\Delta t)^2\big)\right] \tag{10}$$

where f_{md} is the mix-down frequency.

C. Range and Azimuth Resolution

The effective resolution of a SAR image is defined as the half-power width of the impulse response (IPR) [5], which is just the target's appearance in the final SAR image. There are two types of spatial resolution defined for a radar imaging system: range resolution and azimuth resolution. These quantitatively define how closely targets can be spaced in each image direction and still be individually recognized by the radar.

One very common metric for range resolution is called Rayleigh resolution, which is defined as the separation between the peak and the first null of the matched filter response [3]. The Rayleigh range resolution of a pulsed waveform can be expressed as

$$\Delta x = \frac{c}{2\beta} = \frac{c\tau}{2}, \tag{11}$$

where β is the signal bandwidth [3]. If the distance in range between two scatterers is greater than Δx, the radar will receive distinct signal returns from each and we say that the targets are resolved. If not, their signal echoes interfere with each other and cannot necessarily be accurately separated.

The Fourier uncertainty principle [6] states for a given signal that

$$\sigma_t \sigma_w \geq \frac{1}{2}, \tag{12}$$

where σ_t and σ_w are the standard deviations of the pulse duration and the signal bandwidth, respectively. A common interpretation of the uncertainty principle is that a signal cannot have both narrow bandwidth and short pulse duration. This provides the foundation for the relationship $\frac{1}{\beta} = \tau$ between LFM and ICW signals seen in Eq. (11).

Since its range resolution is directly related to pulse duration, ICW radar benefits from very short pulses (low duty cycle). However, SNR requirements necessitate more transmit power, which means transmitting a longer pulse. Since these two ICW system requirements conflict where LFM systems do not, LFM signals are generally preferred to ICW ones. Furthermore, LFM signals can be lengthened for the sake of higher average power without degrading range resolution since it is only dependent on the range of frequencies swept by the signal chirp.

The azimuth resolution Δy of a real aperture radar imaging system is given by

$$\Delta y = \theta_3 R, \tag{13}$$

where θ_3 is the antenna's horizontal 3 dB beamwidth (Eq. (17)) and R is the slant range to the target [5]. This means that the best resolution in real aperture radars is achieved with the narrowest beamwidth (long antenna) and closest range to the target possible. These design specifications severely limit the use and performance of real aperture systems. However, Eq. (13) can be related to the SAR system model by substituting the synthetic aperture beamwidth for θ_3.

The synthetic aperture along-track beamwidth θ_{3s} is given by [5]

$$\theta_{3s} = \frac{\lambda\alpha}{2L_s}, \tag{14}$$

where L_s is the maximum length of the synthetic aperture and is equal to $\theta_3 R$. Substituting Eq. (14), L_s, and subsequently Eq. (17) into Eq. (13) gives

$$\Delta y_s = \theta_{3s} R = \frac{\lambda\alpha R}{2L_s} = \frac{\lambda\alpha R}{2\theta_3 R} = \frac{\lambda\alpha R}{2\frac{\lambda\alpha}{L}R}. \tag{15}$$

After simplifying, this equation becomes

$$\Delta y_s = \frac{L}{2}. \tag{16}$$

Here, we introduce one of the most important properties of SAR imaging systems: that the azimuth resolution is independent of the carrier wavelength and range to the target. Thus, we can achieve incredibly-fine resolution images just by using a smaller antenna.

D. Antenna Design

Part of what makes SAR so versatile is its ability to produce fine-resolution images without the use of a long antenna. In fact, many SAR systems are intentionally designed to utilize a very short antenna, but a SAR antenna that is too small will suffer from degraded SNR.

According to [3], an antenna's beamwidth is inversely proportional to its size. The antenna's beamwidth is generally understood to mean the angular width of the main lobe's radiation pattern at half power as shown in Fig. 4. This is often referred to as the 3 dB beamwidth θ_3 and is given by

$$\theta_3 = \frac{\lambda\alpha}{L}\text{radians}, \tag{17}$$

where α is a constant factor dependent on the antenna's physical properties and L is the length of the antenna. According to Eq. (17), the smaller the antenna, the larger the beamwidth.

SAR systems often use an antenna with a wide beamwidth in order to maximize the amount of time a target spends in the antenna's beamwidth. This is called the dwell time, and in SAR it is often used interchangeably with the coherent processing interval (CPI). Traditionally, the CPI is the number of pulses used for target detection but in SAR, the CPI or dwell time T_d is the time spent imaging a single pixel, given by [3]

$$T_d = \text{dwell time} = n_p \cdot PRI. \tag{18}$$

The CPI is generally equivalent to the time required for the radar platform to cover the length of the synthetic aperture.

One metric used to characterize an antenna's performance is directivity. An antenna's directivity is defined as the ratio of radiation intensity in a reference direction to the average radiation intensity [8]. The reference direction is usually in the direction of maximum radiation. Essentially, it tells us where the antenna concentrates transmitted and received power. Directivity D is directly related to the physical size of the antenna A and is given by [8]

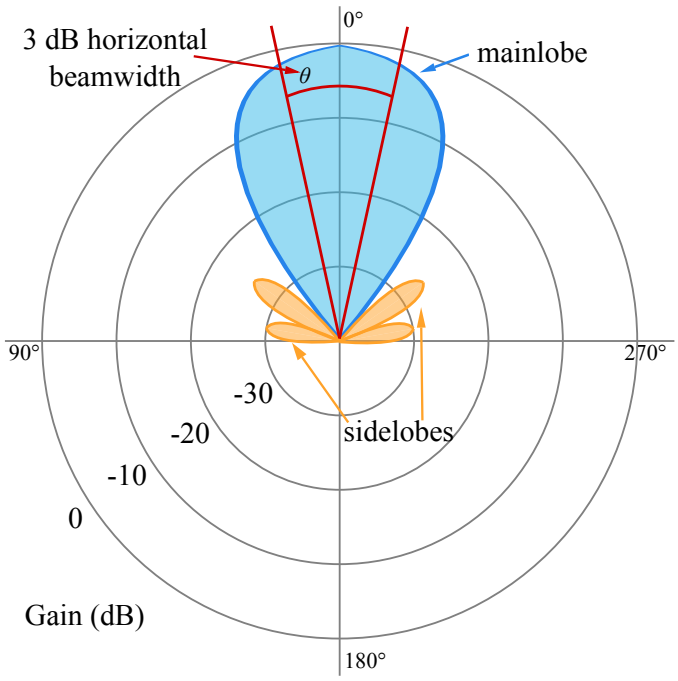

Fig. 4. Typical antenna radiation pattern. Copyright Creative Commons, adapted from [7].

$$D = \frac{4\pi}{\Omega_A}, \tag{19}$$

where Ω_A is the beam solid angle, and is given by

$$\Omega_A = \int\int_{\text{sphere}} |F(\theta,\phi)|^2 \, d\Omega, \tag{20}$$

where $F(\theta,\phi)$ is the normalized electric field pattern. If all power emitted by the antenna were concentrated in a cone at the antenna's maximum radiation and constant distribution, the cone would span a solid angle Ω_A. The familiar gain term G in Eq. (1) is just the maximum directivity minus internal antenna losses.

E. Radar Cross-Section

Beyond the SAR platform itself, there are external factors that affect the received signal intensity. Most importantly, the radar cross-section (RCS) of the targets in the scene of interest tells us how large a target appears to the radar. As opposed to physically-large objects that are easily detectable by human sight, RCS is a measure of a target's electromagnetically reflective strength [9], which depends not only on its physical size, but on its shape and material properties as well.

A point target is a target with small physical dimensions relative to the radar's imaging resolution, but some point targets can have a very high RCS. Consider, for instance, a trihedral corner reflector, as shown in Fig. 5. Corner reflectors are simple targets with known RCS that can be generalized as

$$\sigma = 4\pi A_{\text{eff}}^2/\lambda^2, \tag{21}$$

where A_{eff} is physical area of the corner reflector that participates in the multiple-bounce mechanism. The corner reflector

in Fig. 5 has an A_{eff} of $a^2/2\sqrt{3}$ and an RCS of $\pi a^4/3\lambda^2$ [10]. In this paper, the targets used in simulation behave similar to corner reflectors.

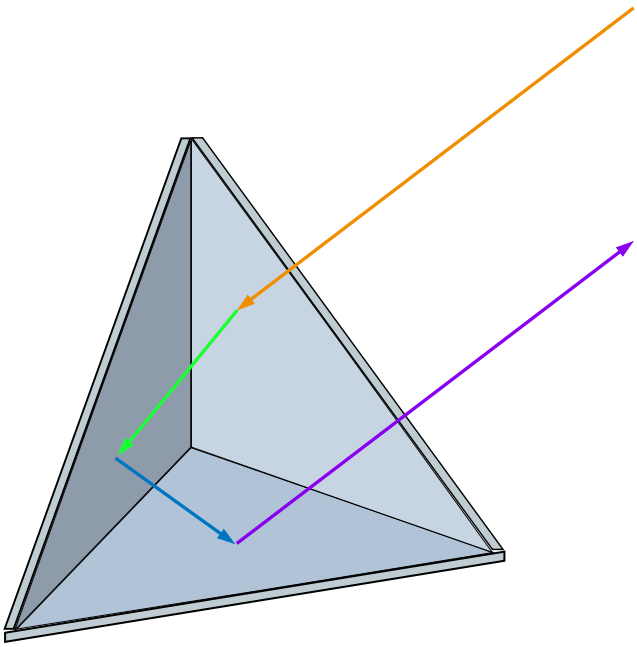

Fig. 5. A trihedral corner reflector. The design of three mutually-orthogonal sides makes this an exceptional radar imaging target. Any incident signal will be reflected directly towards the source. Dihedral corner reflectors are quite prevalent in real-world data when imaging man-made structures and vehicles.

Mathematically, the RCS σ of any target can be expressed as

$$\sigma = \lim_{R\to\infty} 4\pi R^2 \frac{\left|\mathbf{E}^{scat}\right|^2}{\left|\mathbf{E}^{inc}\right|^2}, \tag{22}$$

where $\mathbf{E}^{scat}$ is the scattered electric field and $\mathbf{E}^{inc}$ is the electric field incident at the target [9].

F. Image Formation

When the radar collects data, it is stored as samples of signal amplitude and phase. We must compress the data in both range and azimuth and compensate for range cell migration in order to form an image out of it.

The most common SAR processing algorithms are the range Doppler algorithm (RDA–frequency domain), the chirp scaling algorithm (CSA–frequency domain), the omega-K algorithm (ωKA–2-D frequency domain), and the backprojection algorithm (time domain). Each of these algorithms has processing shortcomings that will be briefly explained in this section.

RDA is the most commonly-used SAR processing method because it has simple implementation and is efficient and relatively accurate. However, it requires computationally-expensive interpolation to correct range cell migration. CSA was developed as an alternative to RDA and uses a more efficient method of range cell migration correction. In order to optimize processing, both RDA and CSA discard higher-order terms of the Taylor series approximation of the SAR signal and are therefore unable to accurately process wide-beam SAR data [11]. While the omega-K algorithm (ωKA) does not make SAR signal model approximations, it assumes constant radar platform velocity, which introduces errors resulting from non-linearities in the aircraft's flight path.

Backprojection is a time-domain azimuth compression algorithm that is computationally expensive but exact. Because backprojection makes no approximations it circumvents problems from SAR geometry that are common in frequency-domain methods, including wide antenna beamwidths and non-linearities in the aircraft's flight path [4]. Backprojection is the most computationally expensive algorithm of those discussed here, but recent developments in GPU computing has almost entirely removed its computational cost. This paper deals exclusively with the backprojection algorithm.

In general, range compression and backprojection are applied to SAR data under the assumption that the either the radar platform or the targets are stationary. For pulsed SAR, a good approximation of platform motion is the stop and hop approximation. This means that the aircraft is assumed to be stationary between transmit and receive pulses. With small PRFs or very long pulse durations this approximation can cause phase estimation errors and image anomalies, but it is a reasonable approximation for pulsed SAR since the movement of the platform from pulse to pulse is negligible compared to the range to the target [12].

1) Range Compression: The matched filter is the optimal linear filter for maximizing SNR of a signal. It requires a received signal and a reference signal. The reference signal is used to extract target features in the imaging scene by measuring differences between it and the received signal. To perform range compression, the matched filter is implemented by applying an FFT to each radar echo, performing a complex multiply between the echo and the complex conjugate of the reference signal, and applying an IFFT to the product. In other words, it is a cross-correlation between transmitted and received signals. Fig. 6 depicts a simple diagram of how to implement range compression in SAR.

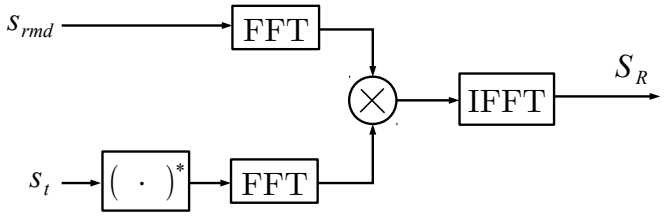

Fig. 6. Block diagram showing the steps of range compression.

As the name implies, range compression compresses SAR data in fast time and gives a one dimensional view of the target scene for any one position in slow time. This is done for every pulse in the data collection, at which point we can perform azimuth compression. Range-compressed data is depicted in Fig. 7, where the range to the target varies hyperbolically, as indicated by the shape of the range migration curve.

2) Range Cell Migration Correction: With wide antenna beamwidths, the dwell time on a particular pixel can be long

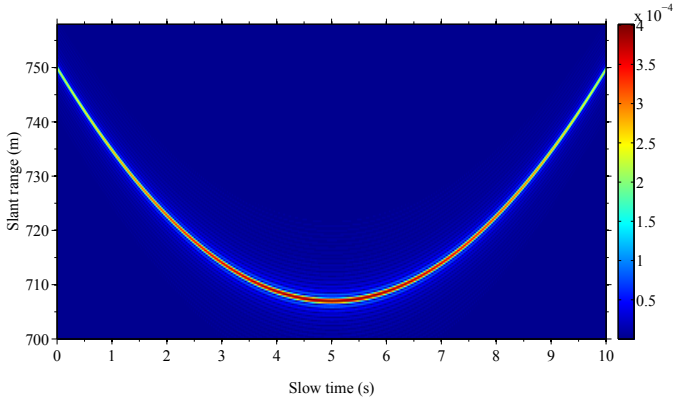

Fig. 7. Range-compressed data for a stationary target 500 meters away from the flight path for a radar platform altitude of 500 meters. Image courtesy Joe Winkler [2]. Used with permission.

enough that the range to that pixel changes more than one range resolution cell Δx throughout the collection. Since all the data across the synthetic aperture is used to form the final SAR image, the target will appear to move through multiple range bins, which is called range cell migration (RCM). RCM complicates image focusing and in general, must be compensated for to produce a focused image. Each SAR processing algorithm approaches range cell migration correction in a different way. For example, the range-Doppler algorithm (RDA) corrects for RCM by applying a frequency-dependent azimuth interpolation to straighten each pixel trajectory so its energy lies in one range bin. On the other hand, the chirp scaling algorithm (CSA) compensates for RCM without interpolation by using chirp scaling functions [12].

3) Azimuth Compression: Azimuth compression is vital to SAR because it coherently sums the data from many positions along a flight path in order to form the synthetic aperture previously discussed. Backprojection is a time-domain azimuth compression algorithm that can compensate for any beamwidth, frequency, or platform motion because it makes no signal, range, or motion approximations. Backprojection uses a matched filter for every pixel in the image by summing the product of the range-compressed data and the complex conjugate of the expected phase. The backprojection equation is given by

$$A(x,y,z) = \sum_{n}^{N} S_R\left(R[x,y,z,n]\right) \cdot \exp\left(\jmath 4\pi R\left[x,y,z,n\right]/\lambda\right), \tag{23}$$

where $A(x,y,z)$ is the complex pixel value at a particular location and S_R is the range-compressed data for a particular range $R[x,y,z,n]$ that has been interpolated to the range of the current pixel. The expected phase of $R[x,y,z,n]$ is $\exp\left(-\jmath 4\pi R\left[x,y,z,n\right]/\lambda\right)$, so Eq. (23) is just the matched filter in slow time.

III. Behavior of Moving Targets in SAR Data

In effect, SAR systems, like digital cameras, take a snapshot in time of a target scene. However, unlike traditional point-and-shoot cameras, SAR systems do not capture data for a single instant in time, but over an extended period of time. In this way, they can be compared to single-lens reflex cameras which often have variable shutter speeds and are used to portray movement and flow when subject focus is not very important. The length of time that a SAR is sending and receiving pulses is called the collection time. In terms of signal-to-noise ratio and image resolution, SAR images benefit most from long collection times. In a photograph of a moving subject, the longer the lens aperture is left open (shutter speed), the more out of focus the subject is. The collection time of a SAR is synonymous with the shutter speed of a camera when a moving target is present in the imaging scene. Hence, moving targets in SAR images are smeared more with longer collection times.

However, moving targets behave very differently in SAR images than they do in optical images. Because SAR is a coherent imaging system, moving targets do not trace out their path in the resulting image. The level and manner of defocusing in SAR images depends on both the magnitude and direction of target motion. In general, a target that has a component of motion in the along-track direction is smeared in that direction, but cross-track target motion causes displacement in the target while preserving image focus.

A. Along-Track Target Motion

A target in a SAR image with an azimuthal component of motion smears in that direction and portrays the general motion of the target [13], [14]. Azimuth smearing results from along-track target velocity, relative radial velocity between the radar and target, and radial target acceleration [15], [16]. The radar's integration angle determines how curved the target smear is. The integration angle is the angle through which the radar moves relative to a single pixel during one coherent processing interval [2]. A SAR system's largest possible integration angle is the 3 dB antenna beamwidth θ_3 and it is common for a SAR to utilize the entire beamwidth for integration in order to realize the best possible azimuth resolution [3].

For a target moving in the along-track direction, the sharpness of its image curve is directly related to the radar's integration angle [2]. The direction of the target relative to the direction of the radar platform determines the orientation of the curve. If the target moves in the same direction as the the aircraft, the hyperbolic image curve is concave out from the aircraft. If the target moves in the direction opposite of the aircraft, the image smear points concave towards the aircraft [13]. The length of the smear is proportional to along-track target speed, as shown in Fig. 8.

B. Cross-Track Target Motion

One might expect cross-track target motion to produce a target smear in SAR images much like along-track motion does. On the contrary, cross-track motion induces much less smearing in the final target image and instead produces a shift in azimuth [13], [15], [17]. In fact, a target with strictly cross-track motion often has so little blurring that it appears as a well-focused stationary target that is shifted in azimuth from

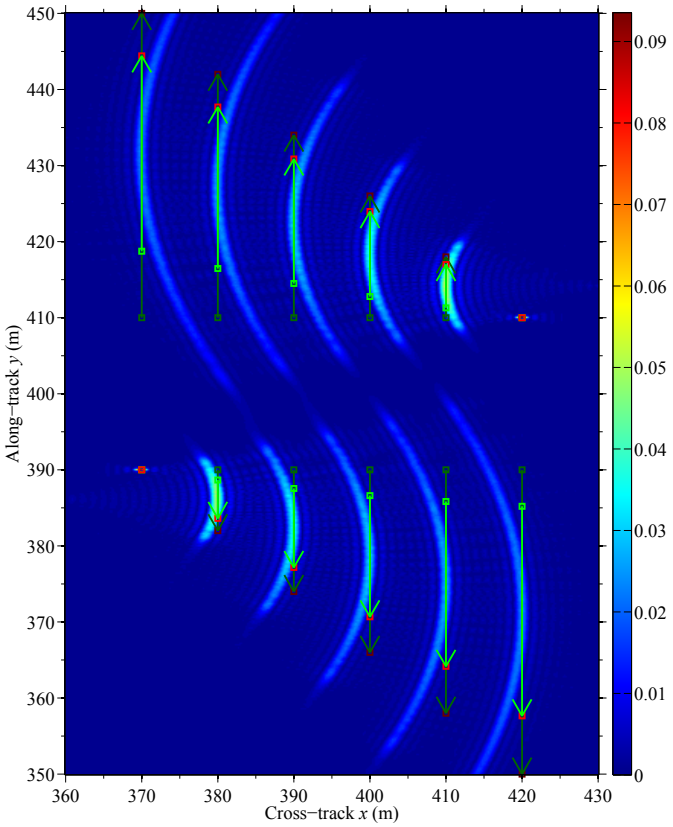

Fig. 8. Simulated SAR image depicting the effects of along-track target motion. The radar platform is moving north at 50 m/s and looks to the right. The top six move in the same direction as the aircraft, and vice versa for the bottom six. The dark green arrows represent each target's path during the radar collection, and the light green arrow represents target motion while it is seen by the antenna. Image courtesy Joe Winkler [2]. Used with permission.

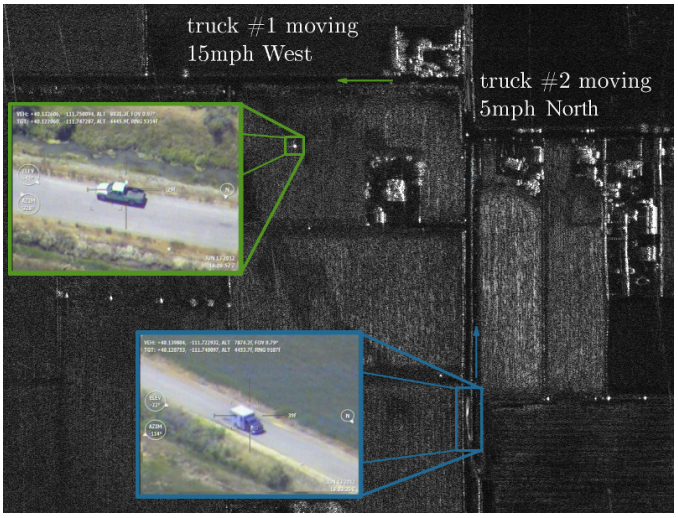

Fig. 9. Actual SAR image of targets moving strictly in range and azimuth with optical images of vehicles overlayed on top of SAR image. The SAR platform is flying North, to the right of the image. Note that the green truck, which moves strictly in the cross-track direction, is well-focused but shifted in azimuth from the road. The blue truck, which has strictly along-track motion, is positioned correctly on the road, but is smeared in azimuth. Image courtesy Artemis, Inc.

its true position. An example of cross track motion is shown in Fig. 9. As shown in Fig. 10, the true position in range is approximately the position of the target half way through the time that it is seen by the antenna's main lobe, which is the target's position at zero Doppler shift. An image of a target that moves towards the flight path of the aircraft shifts in azimuth in the same direction as the aircraft, and vice versa for a target that moves away from the flight path.

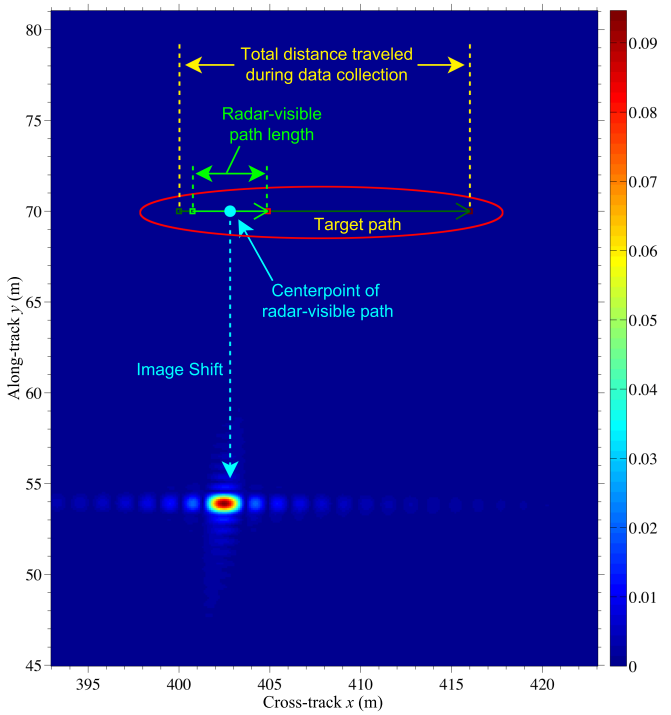

Fig. 10. Simulated SAR image for moving target with only cross-track motion. The radar is positioned to the left of the image, looking to the right. Since the target is moving away from the radar platform, its image is shifted in the opposite direction as the aircraft. The image is shifted approximately below the position of the target when the antenna is broadside to the target, or the zero-Doppler line. Image courtesy Joe Winkler [2]. Used with permission.

The amount of shift in azimuth δx is given by [15]

$$\delta x = \frac{v_r}{v} R \bmod \theta_3 R, \tag{24}$$

where v_r is the target's radial velocity and v is the radar platform velocity. As we can see in Eq. (24), the image shift in azimuth is directly proportional to the radial velocity of the target and range to the target and inversely proportional to the aircraft velocity.

C. GMTI for Single-Channel SAR

In general, SAR signal processing is performed under the assumption that the imaging scene contains only stationary targets. As seen in Eq. (23), in order to produce a fully-focused image, time-domain azimuth compression requires a phase estimate for every image pixel. In single-channel SAR, stationary targets pose no detriment to image formation since the range to an arbitrary stationary target can be known exactly using a signal's two-way time of flight to that target. However,

the exact phase history of moving targets cannot be extracted in single-antenna SAR systems because both the moving radar platform and target contribute to phase changes of a single pixel.

Ground moving target indication (GMTI) can be performed with stationary radars by examining only radar returns with appreciable Doppler shifts. Since the radar is not moving, all stationary targets will have nearly zero Doppler shift and can be ignored. The Doppler shift exhibited by any ground target is given by [3]

$$f_d = \frac{2v_r}{\lambda}, \tag{25}$$

where v_r is the radial velocity of the target relative to the radar platform. Since Doppler shift is literally a measured shift in frequency, we can extract the velocity of a moving target by measuring frequency differences between transmitted and received signals for a particular target.

However, Equation (25) suggests that when the aircraft is moving, all targets exhibit a Doppler shift, and the measured Doppler shift of a given pixel depends on where it is in relation to the radar. Therefore, interfering clutter can come from many different directions and eliminating just the targets with zero Doppler shift is not sufficient in discriminating moving targets from clutter [18].

GMTI can be performed with single-channel SAR if the moving targets have a Doppler shift greater than the Doppler bandwidth of the clutter [1] as given by Eq. (5). However, since the clutter's Doppler bandwidth is proportional to the SAR platform velocity, slow-moving targets cannot be extracted from the clutter because their Doppler shift falls within the clutter bandwidth.

A target's GMTI solution consists of all the parameters necessary to fully characterize the motion of the target, including but not limited to, initial position, heading, speed, and acceleration. In [2], Winkler proves that for uniform SAR platform and target motion, it is mathematically impossible to realize a full GMTI solution based solely on the range migration curve (RMC), an example of which is depicted in Fig. 7. The GMTI solution of a target with uniform motion is given by (x_0, y_0, ψ_t, v_t), where x_0 and y_0 are the target's initial positions in range and azimuth, respectively, ψ_t is the target's heading, and v_t is the target's speed. The RMC can be expressed as a hyperbolic equation [2] in the form of

$$\frac{R^2}{\left(\frac{AC-B^2}{A}\right)} - \frac{\left(t+\frac{B}{A}\right)^2}{\left(\frac{AC-B^2}{A^2}\right)} = 1, \tag{26}$$

where A, B, and C are constants and are defined by the parameters of the GMTI solution. These constants are given by

$$A = v_t^2 \sin^2\psi_t + v_t^2 \cos^2\psi_t - 2v_t v \cos\psi_t + v^2, \tag{27}$$

$$B = x_0 v_t \sin\psi_t + y_0(v_t \cos\psi_t - v), \tag{28}$$

$$C = x_0^2 + y_0^2 + h^2. \tag{29}$$

Since all four GMTI parameters comprise the three hyperbolic function constants, the GMTI solution for single-channel SAR is an underdetermined problem. In [19], Chapman demonstrates that: 1. for every stationary scatterer, there is a set of moving targets at the same range to the radar that to the radar are indistinguishable from each other; and 2. for any moving target with uniform motion, there exists a second target with different position and velocity but same range from the target that is also indistinguishable from the first target. In single-channel SAR GMTI, this is manifest in the form of many target motion parameters that produce an identical RMC, as shown in Fig. 11.

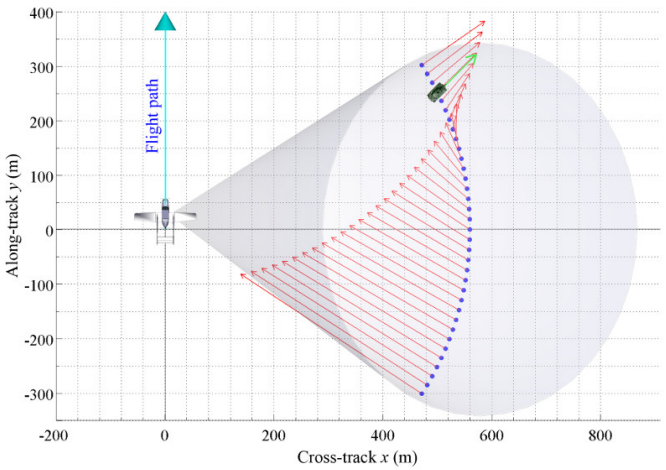

Fig. 11. GMTI solution space for a target moving with GMTI parameters (x_0, y_0, ψ_t, v_t) of (500 m, 250 m, 45°, 10 m/s). The blue dots and corresponding red arrows represent moving target parameters that would all produce identical range history. Length of the arrows is proportional to target speed. Image courtesy Joe Winkler [2]. Used with permission.

D. SAR Ambiguity Function

Backprojection utilizes a 2-D matched filter to maximize image SNR. But when a moving target induces a Doppler shift in the return signal in addition to that caused by the motion of the radar platform, the return signal is mismatched to the filter and the output is lower than its maximum value. An ambiguity function (AF) is a way to characterize the response of the matched filter [3].

In order to show that the GMTI solution for a target with uniform motion for single-channel SAR is underdetermined, I took the following approach. Consider a single simulated SAR collection in a noise- and clutter-free environment. The only non-zero pixels in the final image come from the target's impulse response. The one target in the simulated data moves at a constant heading and speed. During the backprojection algorithm, the target motion can be compensated for by shifting the target pixels according to target's motion. If the wrong motion parameters are chosen, the general result is a defocused image of the target. However, suppose we process the data with compensation for all possible target headings and speeds, each to some arbitrary precision. We then have a large data set of SAR images with different levels of image focus quality. For each image, find the pixel value with the largest magnitude and map that set of values on a 3-D grid

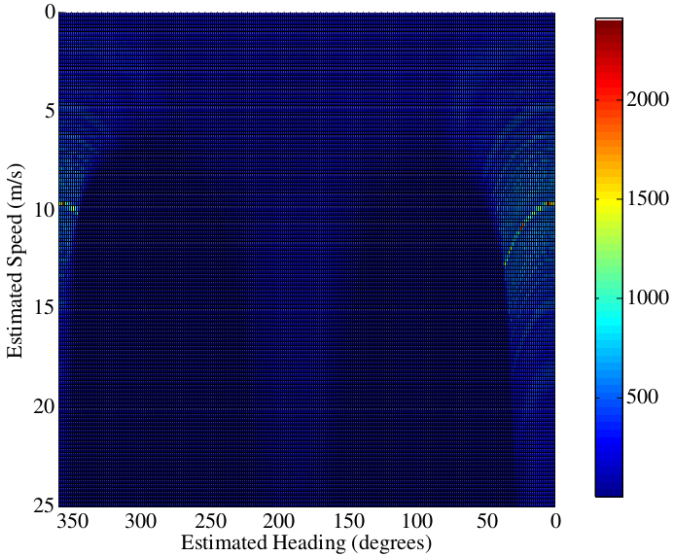

Fig. 12. Top-down view of ambiguity function plotted for a single simulated SAR collection as a function of estimated target heading and speed. These parameters are compensated for during backprojection and each value in the ambiguity function's image is the peak IPR magnitude for some combination of target heading and speed. There is ridge of peak values starting on the left side of the image at about 10 m/s that wraps around to the right side of the image. I call this the ambiguity curve, since it represents motion parameter combinations that produce indistinguishable SAR images. The two parabolic sections with zero intensity represent motion parameter compensation that caused the target to shift completely out of the imaging window.

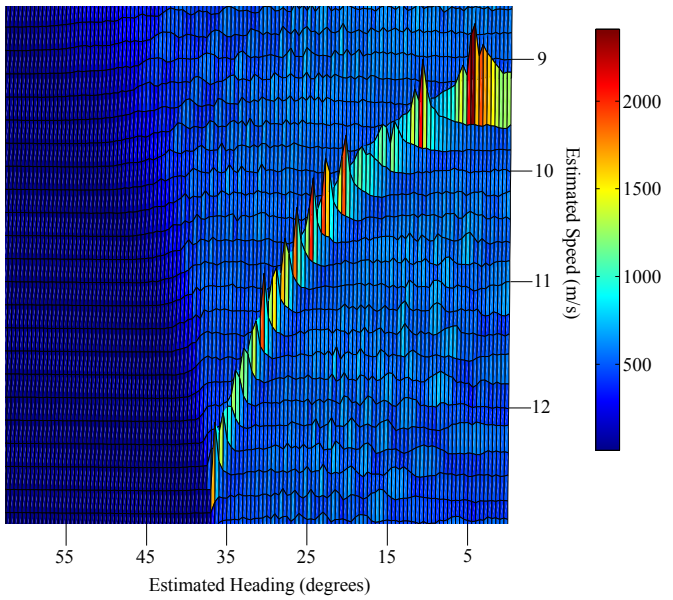

Fig. 13. 3-D view of Fig. 12's ambiguity curve. The peaks of this curve represent motion parameters combinations that produce generally SAR images that are indistinguishable when applied to the same set of data.

with axes for the applied compensation to target heading and speed. The result can be seen in Fig. 12.

The conventional AF is plotted on a grid of Doppler shift and time delay [17]. However, because Fig. 12 depicts SNR as a function of parameter matching, it can be considered an ambiguity function. Since image focus and IPR peak value are generally functions of applied motion compensation, this AF shows the most probable correct motion parameters.

The most important feature of Fig. 12 is the ridge that is seen near the edges of the figure. I call this an ambiguity curve (AC) and give a better perspective in Fig. 13. These peaks in the image occur from the target IPR, which will vary based on the accuracy of the applied motion compensation. It is important to note that in general, the true target motion parameters (15°, 10 meters/second) do not give an impulse any higher than the mean intensity level of the ridge[1]. In fact, each peak represents a combination of motion parameters that produce images that are indistinguishable from each other and all have high IPR values. As an example, consider Table I. In this image, I have plotted 20 different combinations of motion that produce nearly identical image focus. There is slight rotation that is proportional to the error in the estimated target heading and side lobe level variation among the images, but in general, there is little to distinguish these images from each other, especially in regards to image focus.

Let us now consider image focus from a quantitative perspective. One of the most common metrics for image focus is measuring the contrast ratio of the impulse response. Contrast ratio is often defined as the ratio of the signal power in the 3 dB width of the main lobe to the power in the side lobes past the first null. I implemented this by summing the pixel intensities within the nearest 3 dB of the IPR center and comparing it to the side lobe power, while ignoring a guard band from 3 dB to the first null. Table II shows a table comparing IPR widths based on varying motion compensation.

[1]In general, tests have shown that low peak values on the ambiguity curve result from straddle loss [3].

TABLE II
MEAN IPR WIDTHS (IN PIXELS) IN RANGE AND AZIMUTH OVER ALL TEN TARGETS FOR VARIOUS SETS OF APPLIED MOTION COMPENSATION. VALUES HERE CORRESPOND TO THE IMAGES SHOWN IN TABLE I.

3 dB (Range)	3 dB (Azimuth)	Heading	Speed
106.2	7.1	4.5	9.6
109.2	7.6	356.0	9.6
111.1	8.9	30.5	11.6
113.3	7.5	355.0	9.6
117.3	7.9	11.0	9.8
118.1	7.8	15.0	10.0
120.8	7.9	3.5	9.6
123.0	8.4	20.5	10.4
127.3	8.9	24.5	10.8
131.9	9.2	28.0	11.2
132.2	9.4	26.5	11.0
133.7	9.1	18.5	10.2
134.6	8.9	23.0	10.6
135.2	10.1	31.5	11.8
140.7	10.7	29.0	11.4
141.9	12.8	34.0	12.2
142.6	8.7	357.5	9.6
149.1	14.0	33.0	12.0
162.6	10.1	354.0	9.6
168.1	10.5	6.0	9.6

As seen in Table II, there are several sets of motion parameters that produce images as well-focused as the true motion parameters. The existence of motion parameters that produce narrower IPR widths than the true motion parameters demonstrates a weakness of the implemented method of measuring contrast ratio. Because it measures width in range and azimuth and because incorrect heading estimates rotate the final image, the measured IPR width for some motion parameters will be less than that of the true motion parameters. Each line in Table II represents a peak in the AC shown in Fig. 13. As expected, each image corresponding to a peak on the AC has an image that has similar image focus quality.

As a matter of further investigation, let us assume that we can extract motion parameters based on image focus. Consider two SAR images from this simulated collection processed with the true motion parameters and with incorrect motion parameters providing the best quantitative image focus (4.5°, 9.6 meters/second). These are plotted side-by-side in Fig. 14 for comparison. They are nearly indistinguishable, and qualitatively, the image processed with the wrong motion parameters could be said to appear more focused than that of the true motion parameters. The only real differences are the asymmetric side lobes (left) and the rotation of the entire set of targets (right).

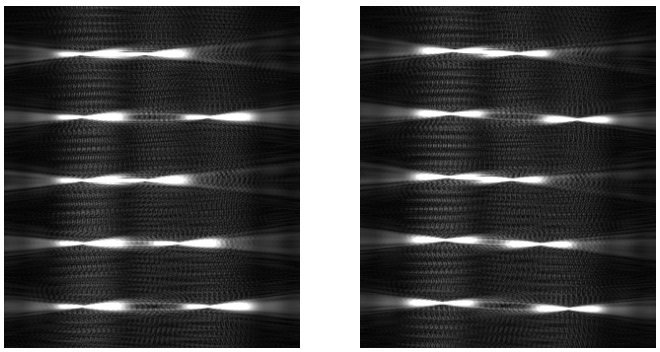

(a) 15°, 10 m/s (b) 4.5°, 9.6 m/s

Fig. 14. Images of simulated SAR data processed with the true motion parameters (left) and incorrect motion parameters (right). Note that the images are nearly identical in image focus and intensity.

The preceding discussion, table, and figures demonstrate the class of moving targets described by Chapman in [19], where several target motion parameter combinations can be used in processing that make the final image indistinguishable from the correct parameters. This chapter has shown that the single-channel SAR GMTI solution is underdetermined. This motivates us to constrain the problem so the GMTI solution is attainable.

IV. Estimating Target Motion Parameters for Uniform Motion

We know that if a target moves uniformly, four parameters can completely characterize its motion, namely position x_0 and y_0, heading ψ_t and speed v_t. Since the RMC of single-channel SAR provides only enough information to extract three of the four GMTI parameters, there is an infinite number of GMTI solutions for any given moving target in single-channel SAR. If we make one of the parameters a constant, the GMTI solution becomes unique and it becomes possible to solve for the true motion parameters using single-channel SAR data.

Considering all four motion parameters of a uniformly-moving target, the most likely constant parameter for a moving target is heading. Since many ground targets of interest move on paved roads, for this chapter we assume that the targets of interest are traveling on straight roads. If the target heading ψ_t is a known constant, this reduces the number of unknowns in Eqs. (27) to (29) to three. We can then solve for x_0, y_0, and v_t exactly.

In [2], Winkler approaches the GMTI problem using the range migration curve. I take a different approach in this paper and in this chapter present a practical method of extracting the exact motion parameters using the AF shown in Fig. 12. This AF is in a different form than a typical AF, in that it is plotted on a grid of heading and speed as opposed to Doppler shift and time delay. However, it still indicates the level of mismatch between the return signal and the filter.

Let's start with some raw SAR data. Image (a) of Fig. 15 shows an image of simulated SAR data. There are ten stationary targets formed in the shape of an 'R'. Now suppose the targets move throughout the SAR collection as one rigid body. In this case, the target moves with a heading of 15° at 10 m/s. This motion is constant throughout the data collection. As discussed in Section III, the target will smear and shift in azimuth because of its motion as seen in (b) on the right.

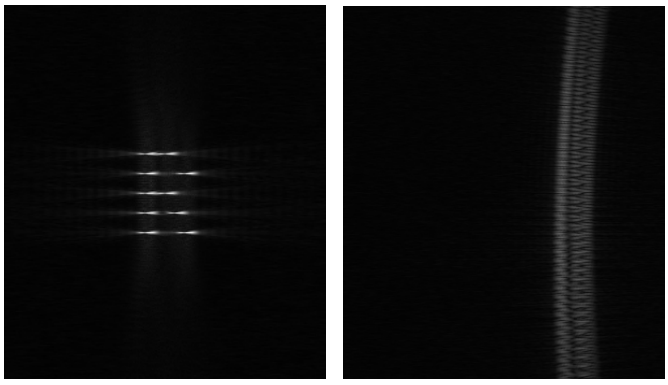

(a) stationary (b) moving

Fig. 15. Images of simulated SAR data. On the left is a set of stationary targets, and on the right, a set of targets moving at 15° and 10 m/s with no applied compensation for target motion.

We now have a defocused image due to motion and would like to focus it. How can we determine the correct motion parameters in order to focus the image in a reasonable amount of time? For clarity in explanation, we must mention backprojection efficiency here. Backprojection is inherently a computationally expensive process because there are $M \times N \times P$ operations to perform for every image, where $M \times N$ is the number of pixels in the image and P is the number of pulses in the data collection. A serial approach to backprojection is extremely inefficient and can take days, or even weeks for a single image. Recently, graphics card manufacturers like NVIDIA have made graphics processing units with many cores

(more than 3000) on each chip [20]. Each of these chips can have hundreds of single precision units, double precision units, special function units for trigonometric operations, and memory registers. This makes these GPUs ideal for parallelizable operations.

The backprojection algorithm can efficiently take advantage of all those cores and decrease the time required to process SAR data by multiple orders of magnitude [4]. All of the SAR processing done in this paper was performed using NVIDIA GPUs. When the task was especially computationally demanding, a high-end NVIDIA GeForce GTX 690 [20] was used.

Let's assume that the target of interest is moving uniformly with unknown speed but that it is traveling on a straight road. These are reasonable assumptions for any ground-moving vehicle in any urban environment. Given this knowledge, the target heading becomes a known parameter and there are only three parameters for which to solve in the GMTI solution. We start by using the process to form an AF described in Section III-D. Since we know the general heading of the road, we process only a section of the full AF based on a range of headings and estimated velocities, which significantly reduces the total processing time. It is important to note that since we have *a priori* knowledge of the target heading because it is on a straight road, this case never calls for us to process a full AF. Even a conservative estimate with large variance in target heading ($\pm$ 10°) and speed (0 – 25 m/s) reduces the processing time by a factor of twenty. The precision between heading and velocity estimates can be adjusted based on the desired AF grid spacing.

Then each image is processed in MATLAB and the maximum value is copied from the image. Since we are working with noise- and clutter-free simulated data, it is safe to assume that the target IPR will contain the maximum value. The peak IPR values are saved and are plotted on a grid that varies with heading and speed estimates used in processing. An example of this is shown in Fig. 16.

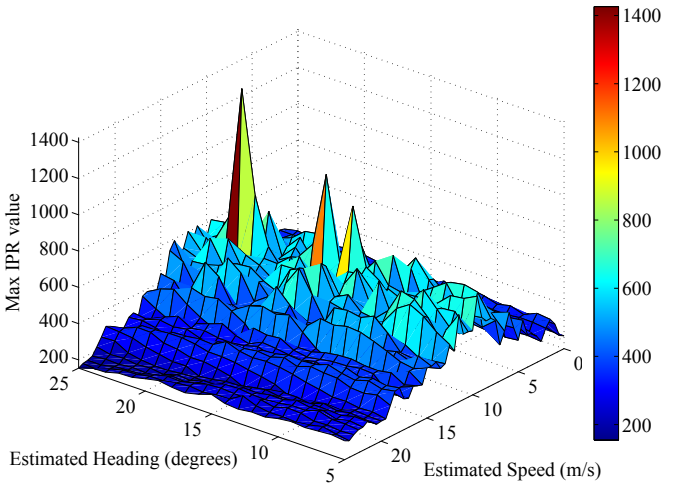

Fig. 16. AF plotted over just a small range of expected values of target heading and speed for efficient processing. The peaks in the image correspond to the peaks in the ambiguity curve in Fig. 12.

Examining the AC, we see that there are many combinations of heading and speed estimates that give a peak in the AF. Since there is generally a strong correlation between image focus and IPR peak magnitude, these peaks indicate the most likely true motion parameter combination.

Most likely, a coarse AF grid is chosen for the first round of processing just so we have an idea of where to give our attention. Looking at Fig. 16, it is apparent that for the known target heading, target speed is fairly consistent with varying heading. If greater accuracy is desired or if straddle loss is encountered (Fig. 17), we can decrease the AF grid size to just a few degrees in heading and a few meter/second in speed, as shown in Fig. 18[2].

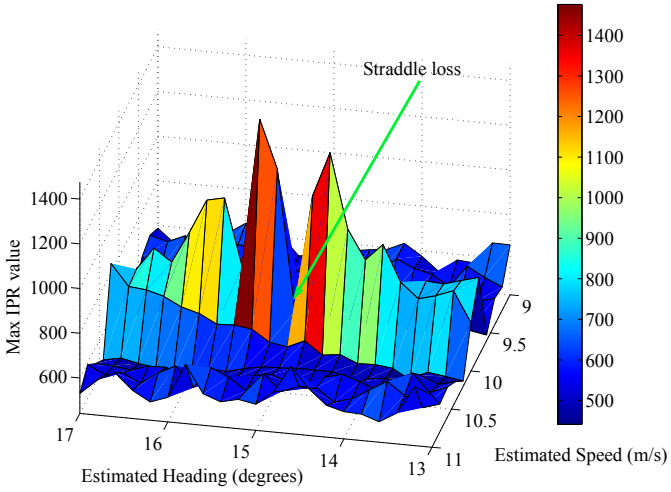

Fig. 17. Ambiguity function suffering from straddle loss because the pixel spacing used when processing the SAR data is too large. Decreasing the pixel spacing gives the finer grid necessary to determine the strongest IPR (and subsequently, the target motion parameters), as shown in Fig. 18.

Finding the peak of the AF shown in Fig. 18 gives us the true target motion parameters. Applying these to the SAR data introduced at the beginning of the section restores image (b) of Fig. 15's focus and produces an image that looks identical to image (a).

V. Conclusion

In this paper, I have presented a feasible method of target motion parameter extraction in single-channel SAR. Even if the initial constraining estimate of target heading is inaccurate to within approximately $\pm$ 5°, since variance in the speed parameter is very low near the true motion parameters, the estimated speed will be fairly close to the true target speed (approximately $\pm$ 0.2 m/s). Presently, this method works only for uniform target motion. It works well for simulated data, but a more robust method of determining maximum target IPR values is necessary for actual SAR data. Future work includes estimating constant acceleration, curved motion, and generally complicated motion for ground moving targets, both in simulated and actual SAR data.

[2]Care should be taken when choosing the SAR image pixel spacing to choose the appropriate spacing for the task. In AF processing, if pixel spacing is too large, the SAR images suffer from straddle loss and the IPR peak magnitudes may be lower than expected, as shown in Fig. 17. If the pixel spacing is too small, processing the AF will take more time than is practical.

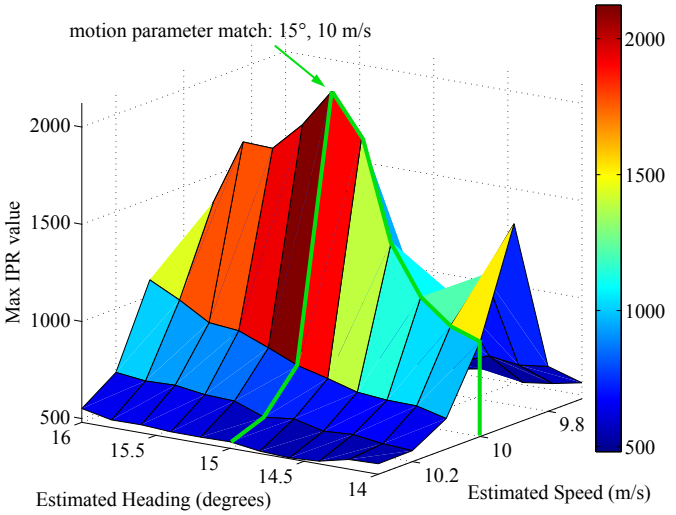

Fig. 18. Finely-sampled ambiguity function with tighter range of heading and speed than Fig. 16. Two lines have been drawn to the peak of the AF to represent the true motion parameters of the moving target. The GMTI solution is given by the intersection of these two lines.

REFERENCES

[1] Merrill I. Skolnik. *Introduction to Radar Systems*. McGraw-Hill, New York, NY, 3rd edition, 2001.

[2] J.W. Winkler. "An Investigation of Ground Moving Target Indication (GMTI) with a Single-Channel SAR System". Master's thesis, Brigham Young University, 2013.

[3] Mark A. Richards, James A. Scheer, and William A. Holm. *Principles of Modern Radar*. SciTech, Edison, NJ, 2010.

[4] E.C. Zaugg. *"Generalized Image Formation for Pulsed and LFM-CW Synthetic Aperture Radar"*. PhD thesis, Brigham Young University, 2010.

[5] Fawwaz T. Ulaby, David G. Long, Adrian K. Fung, and Richard K. Moore. *Microwave Remote Sensing Modern Edition*. Artech House, Norwood, MA, 2013.

[6] P.J. Loughlin and L. Cohen. The uncertainty principle: global, local, or both? *Signal Processing, IEEE Transactions on*, 52(5):1218–1227, May 2004.

[7] Radiation pattern. http://en.wikipedia.org/wiki/Radiation_pattern, February 2014. Accessed: 20 Mar 2014.

[8] Warren L. Stutzman and Gary A. Thiele. *Antenna Theory and Design*. Wiley, Hoboken, NJ, 3rd edition, 1998.

[9] F. Jay, editor. *IEEE Standard Dictionary of Electrical and Electronic Terms*. ANSI/IEEE Std 100-1984. IEEE Press, New York, NY, 3rd edition, 1984.

[10] Eugene F. Knott, Michael T. Tuley, and John F. Shaeffer. *Radar Cross Section*. Artech House, Norwood, MA, 2nd edition, 2004.

[11] I.G. Cumming, Y.L. Neo, and F.H. Wong. Interpretations of the omega-k algorithm and comparisons with other algorithms. In *Geoscience and Remote Sensing Symposium, 2003. IGARSS '03. Proceedings. 2003 IEEE International*, volume 3, pages 1455–1458, July 2003.

[12] Ian G. Cumming and Frank H. Wong. *Digital Processing of Synthetic Aperture Radar Data: Algorithms and Implementation*. Artech House, Norwood, MA, 2005.

[13] Jen King Jao. Theory of synthetic aperture radar imaging of a moving target. *Geoscience and Remote Sensing, IEEE Transactions on*, 39(9):1984–1992, Sep 2001.

[14] M. Kirscht. Detection and imaging of arbitrarily moving targets with single-channel sar. In *RADAR 2002*, pages 280–285, Oct 2002.

[15] R.K. Raney. Synthetic aperture imaging radar and moving targets. *Aerospace and Electronic Systems, IEEE Transactions on*, AES-7(3):499–505, May 1971.

[16] S. Barbarossa. Detection and imaging of moving objects with synthetic aperture radar. 1. optimal detection and parameter estimation theory. *Radar and Signal Processing, IEE Proceedings F*, 139(1):79–88, Feb 1992.

[17] Victor C. Chen and Hao Ling. *Time-Frequency Transforms for Radar Imaging and Signal Analysis*. Artech House, Boston, MA, 2002.

[18] J. R. Guerci. *Space-Time Adaptive Processing for Radar*. Artech House, Norwood, MA, 2003.

[19] R. D. Chapman, C.M. Hawes, and M. E. Nord. Target motion ambiguities in single-aperture synthetic aperture radar. *Aerospace and Electronic Systems, IEEE Transactions on*, 46(1):459–468, Jan 2010.

[20] Geforce gtx690 specifications. http://www.geforce.com/hardware/desktop-gpus/geforce-gtx-690/specifications, 2014. Accessed: 15 Apr 2014.

TABLE I
20 SAR IMAGES PROCESSED FROM THE SAME SIMULATED SAR DATA WITH VARYING MOTION PARAMETERS. IMAGE FOCUS IS APPROXIMATELY THE SAME BETWEEN ALL IMAGES. TRUE MOTION PARAMETERS ARE 15.0°, 10.0 M/S.